Bioactive Materials 5 (2020) 219–227

Contents lists available at ScienceDirect

Bioactive Materials

journal homepage: http://www.keaipublishing.com/biomat

Effect of extrusion process on the mechanical and in vitro degradation performance of a biomedical Mg-Zn-Y-Nd alloy

Beining Du[a], Ziyang Hu[b], Jiali Wang[c], Liyuan Sheng[a,*], Hui Zhao[d], Yufeng Zheng[a], Tingfei Xi[a]

[a] Shenzhen Institute, Peking University, Shenzhen, 518057, China
[b] Shenzhen Yezhan Electronics Co., Ltd, Shenzhen, 518110, China
[c] School of Biomedical Engineering, Sun Yat-sen University, Guangzhou, 510006, China
[d] School of Materials Science and Engineering, Xi'an Shiyou University, Xi'an, 710065, China

ARTICLE INFO

Keywords:
Mg–Zn–Y-Nd alloy
Microstructure
Tensile property
Degradation performance

ABSTRACT

A new type of biomedical Mg–Zn–Y-Nd alloy was developed and thermal extruded by different processes to investigate the effect of extrusion ratio and extrusion pass on its microstructure, mechanical property and degradation performance. The results show that the increase of extrusion ratio could promote the dynamic recrystallization (DRX) process and led to the coarsening of DRXed grains. While the increase of extrusion pass also contributes to the DRX process but refines the DRXed grains. The simultaneous increasing of extrusion ratio and extrusion pass refines the secondary phases obviously. The increase of extrusion ratio has reduced the tensile strength but improved the elongation of the alloy significantly. However, the increase of extrusion pass could enhance the tensile strength and elongation simultaneously, especially the strength. The degradation performance has been optimized effectively through increasing the extrusion ratio and extrusion pass.

1. Introduction

Magnesium (Mg) alloys have been considered as potential biodegradable orthopedic implant material due to the low density (1.7–2.0 g/cm^3), similar elastic modulus (41–45 GPa) with human bone, relative high stiffness and good biocompatibility [1–5]. However, the insufficient strength and poor plasticity result in the inability of Mg alloys to provide support as orthopedic implants [6,7]. Moreover, the rapid degradation rate in human environment has also handicap their clinical application [7]. Therefore, optimization of the mechanical properties and corrosion resistance has become an urgent demand to promote the medical application of Mg alloys.

Thermal extrusion is one of the most commonly used methods to refine the grains and optimize the microstructure of Mg alloys. It could improve the mechanical properties and corrosion resistance effectively [8,9]. However, the effects of extrusion process on Mg alloys are closely related to the extrusion parameters, such as temperature, extrusion ratio and pass [10]. It is widely recognized that the increase of extrusion temperature would accelerate DRX process and increase the DRXed grain size [11–13]. However, there are different viewpoints on the influence of extrusion ratio on the microstructure of Mg alloys. The investigation of Zhao [14] on the effect of extrusion ratio on the Mg–Zn–Y–Zr alloy has revealed that the increase of extrusion ratio could refine the grains obviously and improve the room temperature mechanical properties effectively. Chen [13,15] has studied the effects of extrusion ratio on the Mg–Zn-RE-Zr alloy and the results show that once the critical minimum grain size is achieved, further increase of extrusion ratio would has little influence on grain refinement and improvement of mechanical properties. However, Zhang has investigated the thermal extruded Mg-Nd-Zn-Zr alloy with different ratios and found that lower extrusion ratio results in finer grains, higher strength but lower elongation, while the higher extrusion ratio results in coarser grains and lower strength [10]. Besides the extrusion temperature and ratio, the extrusion pass is also an important parameter that would influence the microstructure and mechanical properties of the Mg alloys. Multi-pass extrusion is an effective way to optimize the microstructure, mechanical property and corrosion resistance of Mg alloys. The recent study of Tian [16] exhibited that the Mg-1.5Zn-0.25Gd alloy processed by 2, 4 and 8 passes cyclic extrusion obtains yield strength of 288 MPa, 272 MPa, 251 MPa respectively, and the alloy with 8 passes cyclic extrusion process obtained the elongation of 31.4%. Wu [17] has investigated the influence of multi-pass extrusion on a Mg–Zn–Y-Nd alloy for vascular stent application, and the results show that two-pass extrusion could refine the grain size and homogenize the distribution of

Peer review under responsibility of KeAi Communications Co., Ltd.
* Corresponding author.
E-mail addresses: lysheng@yeah.net, bndu10s@alum.imr.ac.cn (L. Sheng).

https://doi.org/10.1016/j.bioactmat.2020.02.002
Received 15 November 2019; Received in revised form 1 February 2020; Accepted 1 February 2020

nano-sized secondary phases, thus enhance the mechanical properties and lead to homogeneous corrosion of the alloy.

In the present study, a new type of Mg–Zn–Y-Nd alloy for degradable orthopedic implants was developed because Zn is an essential element of human body, and the minor rare earth element Y and Nd could refine the microstructure of Mg alloys. After then the Mg–Zn–Y-Nd alloy was thermal extruded at different extrusion ratios and passes. The microstructure, tensile property and degradation performance of the alloy with different extrusion states were investigated. The microstructure evolution, tensile deformation mechanism and degradation mechanism were discussed.

2. Experimental

The investigated alloy with a nominal composition of Mg–4Zn-1.2Y-0.8Nd (wt. %) alloy was melted in an electric resistance furnace under a protection of mixture gas of CO_2 and SF_6 in ratio of 100:1. Alloying elements Zn, Y and Nd were added in the form of pure Zn (100%) and Mg–25Y (wt. %), Mg–25Nd master alloys, respectively. The melts were poured into a mild steel crucible preheated to 200–300 ˚C with a diameter of 150 mm. Then surface machining was used to remove the oxidized layer of the as-cast ingots, and solution heat treatment was applied at 500 ˚C for 2h. After that, these heat treated ingots were divided into three groups and subsequent hot extruded by three different extrusion processing. As shown in Table 1, firstly, the one group of ingots were thermal extruded at 460 ˚C and the extrusion ratio was 7 to obtain alloy E1. Secondly, the two group of ingots were also thermal extruded at 460 ˚C, but the extrusion ratio was 14 to obtain alloy E2. Thirdly, two-pass extrusion was carried out on the last group of ingots to obtain alloy E3. The first pass extrusion was conducted at 460 ˚C with the extrusion ratio of 7, and the second pass extrusion was conducted at 400 ˚C with the extrusion ratio of 12.

The microstructures of alloy E1, E2 and E3 were observed through scanning electron microscope (SEM), and the size and volume fraction of grains and secondary phases of these alloys was calculated through IPP software. Electron Backscattered Diffraction (EBSD) was used to analysis the texture and twins of these alloys. The uniaxial tensile tests were conducted on an INSTRON 5582 testing machine with a speed of 0.1 mm/min at room temperature. The tensile direction was parallel to the extrusion direction (ED). After that, in-situ tensile test was conducted on alloy E1 and E2 to observe the microstructure evolution during the tensile deformation.

The samples for immersion tests were cut into 10 × 10 × 5 mm, and grinded and polished. The samples were immersed in Hank's solution at 37 ˚C for 30 min, 3 h, 8 h, 15 h, 24 h, 50 h, 125 h, 315 h, and 600 h. Before immersion, the samples were weighed through analytical balance and the sizes of the samples were measured through vernier caliper to calculate their surface areas. After immersion for different time, the samples were immersed into 200 g/L CrO_3 + 10 g/L $AgNO_3$ solution for about 10 min to remove the corrosion product on the sample surface, and then the samples were cleaned with ethanol, and dried. After that, the samples were weighed. At last, the morphology and 3D morphology of the specimens after immersion for different time was observed by SEM and Keyence optical microscope.

Table 1
The different extrusion process of these alloys.

Alloy number	Extrusion process: temperature/extrusion ratio
Alloy E1	One-pass extrusion: 460 ˚C/7
Alloy E2	One-pass extrusion: 460 ˚C/14
Alloy E3	Two-pass extrusion: 460 ˚C/7 + 400 ˚C/12

3. Results and discussions

3.1. Microstructure

The microstructures of Mg–Zn–Y-Nd alloys with different states are shown in Fig. 1. It can be found that the as-cast alloy consists of coarse equiaxed grains and continuous secondary phases that distribute along grain boundary. Alloy E1 is composed of small equiaxed grains which could be called DRXed grains and coarse elongated grains which could be called unDRXed grains, while alloy E2 consists of relative coarse equiaxed grains but no elongated grains. Alloy E3 also contains equiaxed grains and elongated grains, but they are all smaller than alloy E1. The major secondary phases are block and granular, and distribute linearly along ED, and there are also some nanoscaled precipitates disperse in these Mg–Zn–Y-Nd alloys.

The volume fraction and average size of the DRXed grains and secondary phases are calculated and the results are shown in Table 2. The volume fraction and average size of DRXed grains of alloy E1 is 68.27% and 6.65 μm, respectively. While the volume fraction and average size of DRXed grains of alloy E2 increase to 100% and 12.78 μm. The volume fraction of DRXed grains of alloy E3 increases to 92.41%, but the average size of DRXed grains decreased to 3.70 μm. Therefore, it can be found that the increase of extrusion ratio could increase the size and volume fraction of DRXed grains, while the increase of extrusion pass would increase the volume fraction but decreased the size of DRXed grains. The volume fraction of secondary phase in alloy E1, E2 and E3 shows little change, but its size in alloy E2 and E3 is both smaller than that in alloy E1.

The microstructure evolution during different thermal extrusion process are shown in the schematic diagram in Fig. 2. During thermal extrusion, the original grains are elongated along ED and form elongated grains [18]. Moreover, dynamic recrystallization would occur and form small equiaxed grains [19]. For alloy E1, the dynamic recrystallization is incomplete and there are still some elongated grains left, as shown in Fig. 2 (a). For alloy E2, it can be found that the dynamic recrystallization is complete and there is no unDRXed grains left. Therefore it can be deduced that the increase of extrusion ratio could promote the dynamic recrystallization process during thermal extrusion. As shown in Fig. 1 and Table 2, the increase of extrusion ratio has increased the DRXed grain size of Mg–Zn–Y-Nd alloy in the present study. There are contradictory results about the effect of extrusion ratio on the grain size of Mg alloys. Chen [20] has reported that the grain size of the AZ31 alloys decreased as the extrusion ration increase. Uematsu [21] has found the same conclusion about AZ61A and AZ80 alloy. However, Hirano [22] claimed that the grain size of Mg97Zn1Y2 alloy increased with increasing extrusion, and Zhang [10] has obtained similar results in Mg-Nd-Zn-Zr alloy. During extrusion process, a larger extrusion ratio means higher deformation strain and stress, which leads to higher deformation energy. It is known that the dynamic recrystallization temperature decreases with the increase of deformation energy [10]. In the present study, as extrusion ratio increasing, the extrusion deformation energy increases, thus the dynamic recrystallization temperature decreases. Therefore the dynamic recrystallization temperature of alloy E2 is lower than that of alloy E1. Since the extrusion temperatures of alloy E1 and E2 are the same, the dynamic recrystallization occurs easier and the DRXed grains grow faster for alloy E2. Therefore alloy E1 exhibits partial dynamic recrystallization and smaller DRXed grains, while alloy E2 exhibits complete dynamic recrystallization and larger DRXed grains, as indicated in Fig. 2 (b).

Comparing alloy E1 and E3, it can be found that the increase of extrusion pass has increased the volume fraction but decreased the size of DRXed grains. In our previous study [18], it has been found that dynamic recrystallization would continue to occur during the second pass of extrusion, hence the unDRXed grains would be further consumed, and the volume fraction of DRXed grains would increase. The

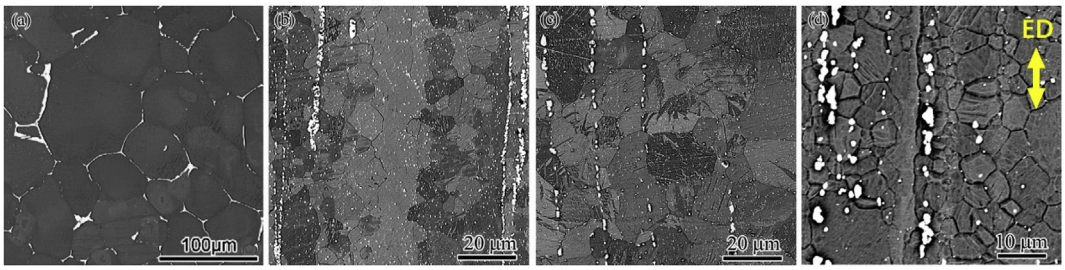

Fig. 1. Microstructure of the Mg–Zn–Y-Nd alloy with different states: (a) As-cast alloy; (b) Alloy E1; (c) Alloy E2; (d) Alloy E3.

Table 2
The volume fraction and average size of the DRXed grains and secondary phases of Mg–Zn–Y-Nd alloys.

Alloys	DRXed grains		Secondary phase	
	Volume fraction	Average size (μm)	Volume fraction	Average size (μm)
E1	68.27% ± 3.53%	6.65 ± 0.48	3.77% ± 0.28%	2.23 ± 0.26
E2	100%	12.78 ± 0.73	3.37% ± 0.45%	1.13 ± 0.39
E3	92.41% ± 2.78%	3.70 ± 0.36	3.66% ± 0.51%	0.80 ± 0.21

second pass of extrusion temperature (400 °C) is lower than the first pass (460 °C).As is reported that decreasing extrusion temperature would result in grain refining [13,15], the DRXed grains formed during the second pass of extrusion are smaller than the first pass. Moreover, sub-boundaries would be produced in the DRXed grains formed during the first pass extrusion, which would divide these DRXed grains into smaller ones, as shown in Fig. 2 (c).

EBSD analysis was conducted on alloy E1, E2 and E3 and the results

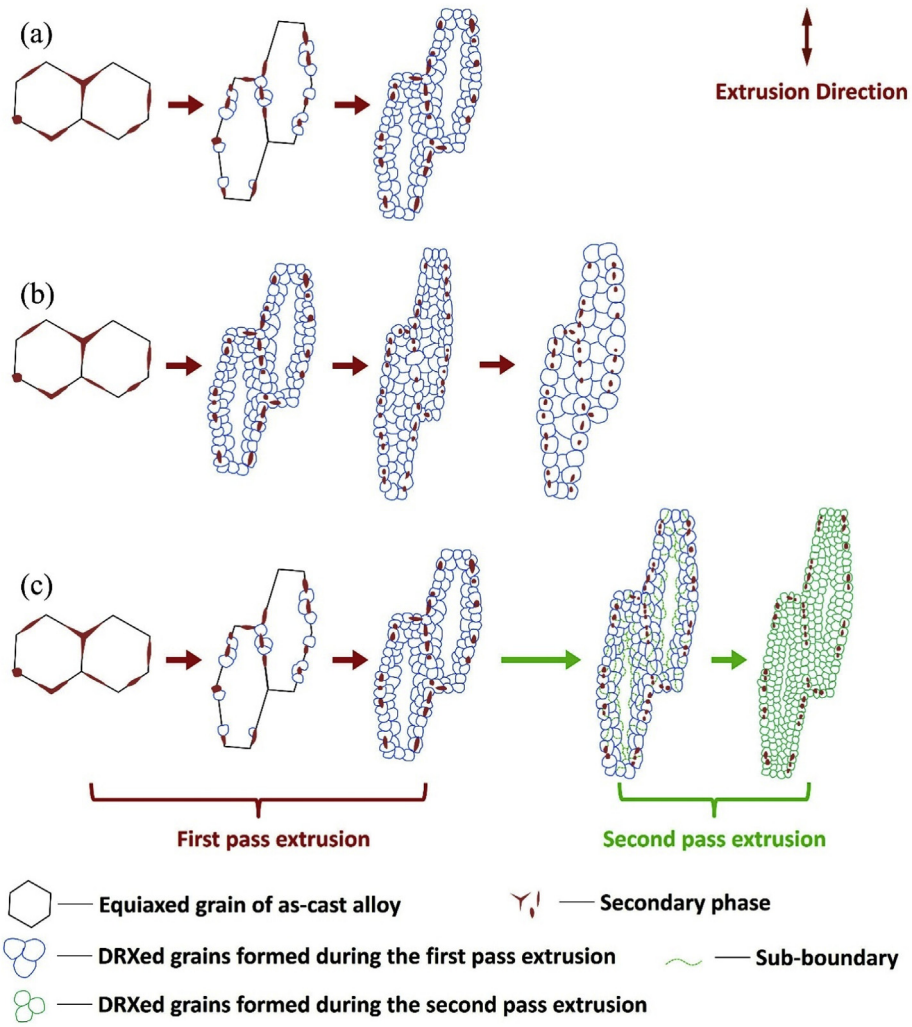

Fig. 2. Schematic diagram of the microstructure evolution during different extrusion process: (a) Alloy E1; (b) Alloy E2; (c) Alloy E3.

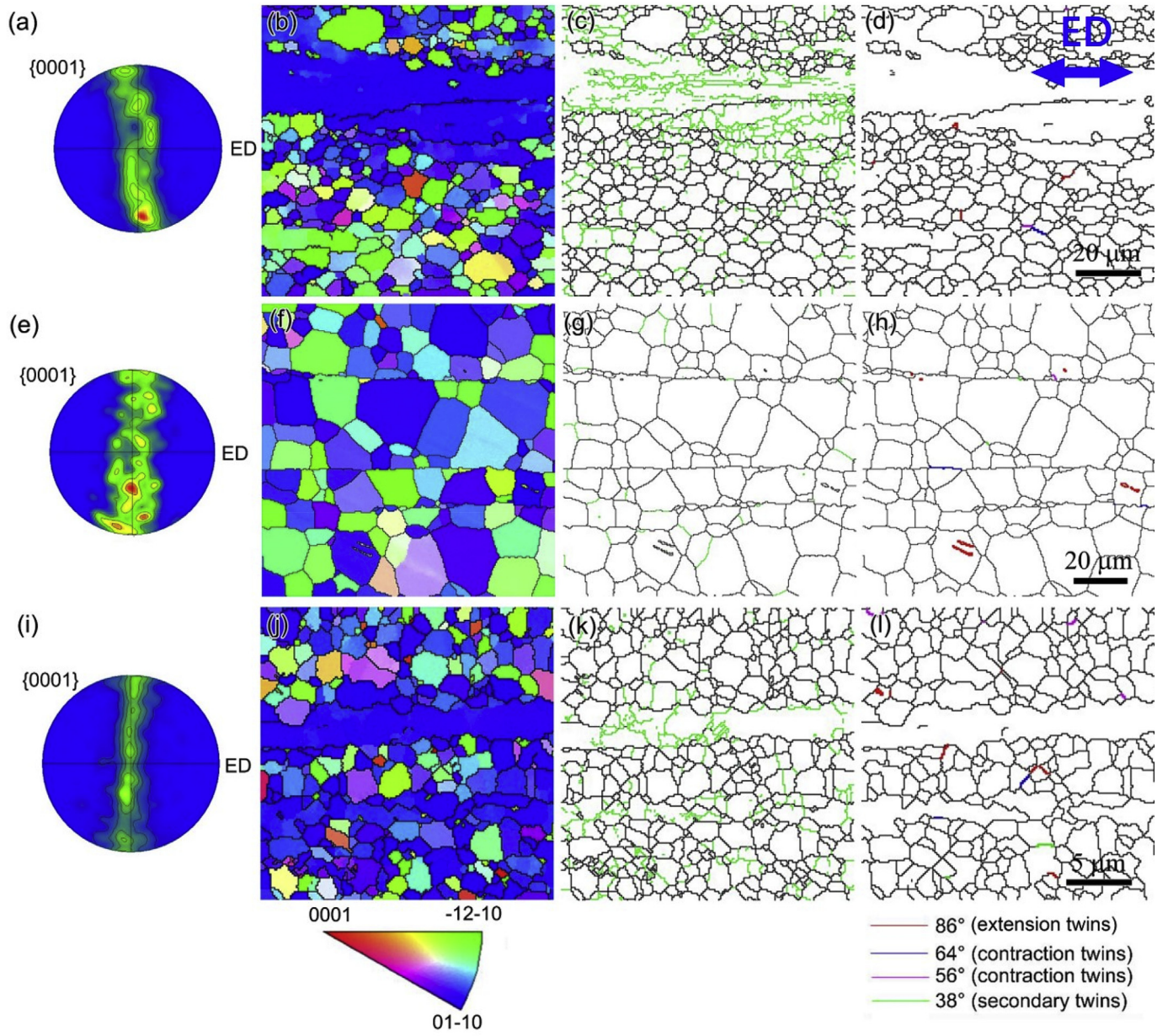

Fig. 3. EBSD results of alloy E1, E2 and E3: (a)–(d) Alloy E1; (e)–(h) Alloy E2; (i)–(l) Alloy E3; (a) (e) (i) Polar figure; (b) (f) (j) Inverse polar figure; (c) (g) (k) Grain boundary map; (d) (h) (l) Twin map. (The black lines in the grain boundary maps represent high angle grain boundaries (HAGBs) and green lines represent low angle grain boundaries (LAGBs)).

are shown in Fig. 3. As shown in the polar figures in Fig. 3 (a), (e) and (i), alloy E1, E2 and E3 all demonstrate strong basal textures that {0001} plane of α-Mg matrix is parallel to ED. Comparatively, the basal texture of alloy E1 is stronger than alloy E2 but weaker than alloy E3. During thermal extrusion, the original grains would be elongated towards ED, and the crystal lattice would rotate in order to coordinate the integral deformation, thus form elongated grains with basal texture, as shown in the IPF of Fig. 3 (b). While the DRXed grains tend to show more random texture. Since the volume fraction of DRXed grains of alloy E2 are much higher than alloy E1, its basal texture is weaker than that of alloy E1. However, comparing alloy E1 and E3, the two-pass extrusion has promoted the basal texture. Although alloy E3 contains a higher DRXed grain volume fraction, it shows stronger basal texture than alloy E1. The grain boundary maps of these three alloys are shown in Fig. 3 (c), (g) and (k). For alloy E1, there are large numbers of low angle grain boundaries (LAGBs) in the elongated grains but only a small amount in the DRXed grains, while there are almost no LAGBs in alloy E2. The LAGBs are caused by the deformation during thermal extrusion. The dynamic recrystallization process would consume the LAGBs, thus there are only a few LAGBs in the DRXed grains. For alloy E3, the elongated grains become thinner, and the LAGB density becomes lower because of the dynamic recrystallization during the second pass of extrusion. The twin maps of these three alloys in Fig. 3 (d), (h) and (l) show that there are only a very small number of twins in all the three alloys, which means that the thermal extrusion process has hardly produced any twins in Mg–Zn–Y-Nd alloy in the present study.

3.2. Tensile property

The tensile tests were carried at room temperature. The tensile properties are shown in Fig. 4. The tensile yield strength (TYS), tensile ultimate strength (TUS) and elongation of alloy E1 are 191 MPa, 258 MPa and 13.3%, respectively. For alloy E2, its TYS and TUS decrease to 138 MPa and 235 MPa, but its elongation increases

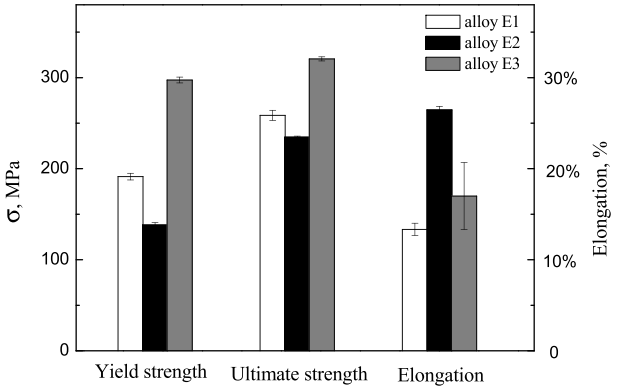

Fig. 4. Tensile properties of alloy E1, E2 and E3.

significantly to 26.5%. While for alloy E3, its TYS and TUS increase greatly to 297 MPa and 320 MPa, and its elongation increases to 17%. Therefore in the present study, the increase of extrusion ratio has decreased the strength, but improved the ductility of Mg–Zn–Y-Nd alloy greatly, which is quite similar with the research of Zhang on a biomedical Mg-Nd-Zn-Zr alloy [10] but inconsistent with the research of Zhao on a Mg–Zn–Y–Zr alloy [14]. According to the above analysis of the microstructure evolution, as the increase of extrusion ratio, the coarsening of recrystallized grains leads to strength decrease, while the uniform grain structure caused by complete recrystallization leads to a large increase in plasticity.

The increase of extrusion pass has improved both the strength and ductility of Mg–Zn–Y-Nd alloy. Different from extrusion ratio, the effects of multi-pass extrusion on the microstructure and mechanical property of Mg alloys are relatively consistent. In the investigation of Tian [16], Wu [17], and our previous study [18], similar results are obtained that the grains and precipitates are refined through multi-pass extrusion because continued dynamic recrystallization, therefore both the strength and ductility could be improved.

After tensile tests, samples were cut from the fractured specimens and EBSD analyses were applied. As shown in the polar figures and inverse polar figures in Fig. 5 (a), (b), (e), (f), (i) and (j), the basal texture is enhanced after tensile tests. For alloy E1, the LAGBs increase significantly after tensile test, especially in the DRXed grains, as shown in Fig. 5 (c). These LAGBs are formed through dislocation segregation at the grain boundaries during tensile test [23]. Moreover, many twins appear in alloy E1 after tensile test, and these twins consist of extension twins (86°), contraction twins (64° and 56°) and secondary twins (38°). Among which contraction twins are the main twins in alloy E1, especially in the DRXed grains, as shown in Fig. 5 (d). As the above analysis, the extruded alloy show basal texture. During tensile test along ED, the

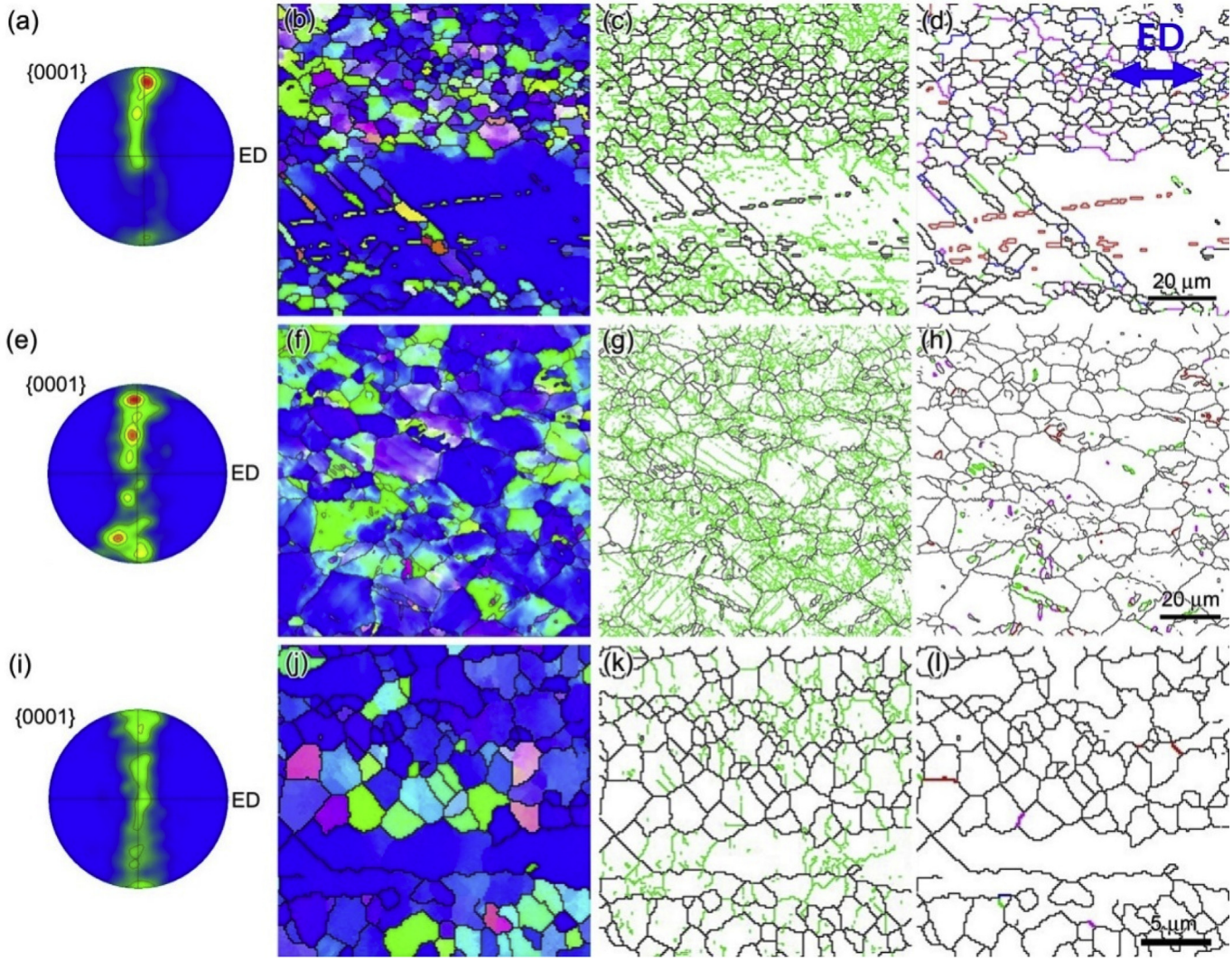

Fig. 5. EBSD results of alloy E1, E2 and E3 after tensile tests: (a)–(d) Alloy E1; (e)–(h) Alloy E2; (i)–(l) Alloy E3; (a) (e) (i) Polar figure; (b) (f) (j) Inverse polar figure; (c) (g) (k) Grain boundary map; (d) (h) (l) Twin map.

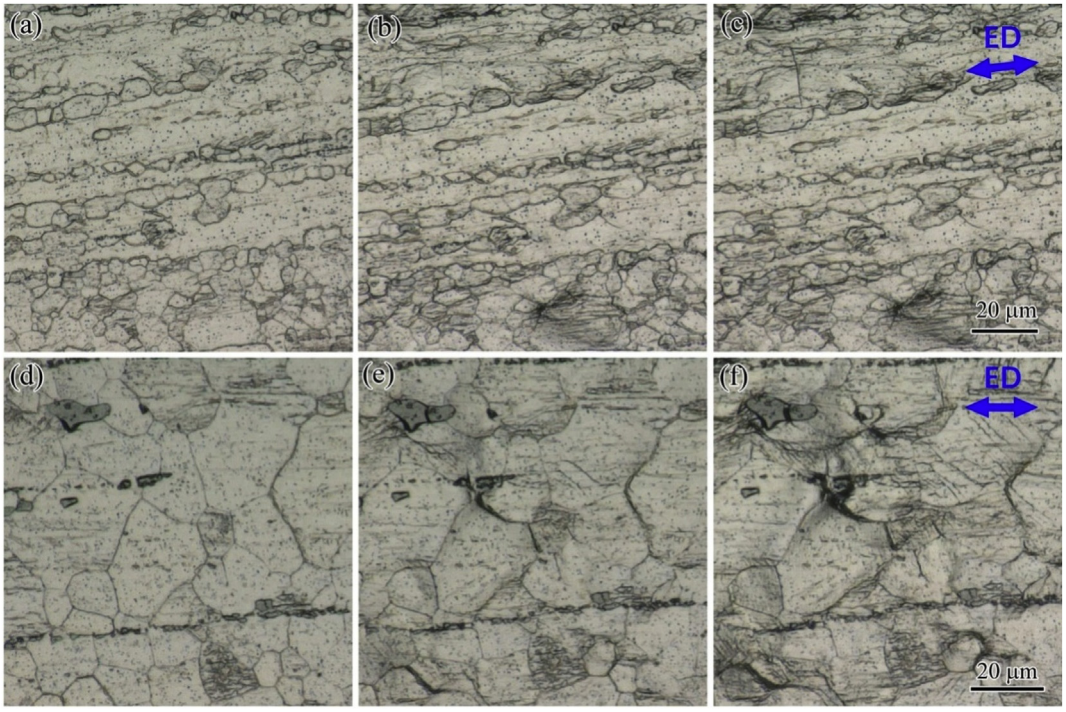

Fig. 6. Microstructure evolution of alloy E1 and E2 during in-situ tensile tests: (a) (b) (c) alloy E1; (d) (e) (f) alloy E2; (a) ε = 2%; (b) ε = 10%; (c) ε = 11%; (d) ε = 2%; (e) ε = 10%; (f) ε = 15%.

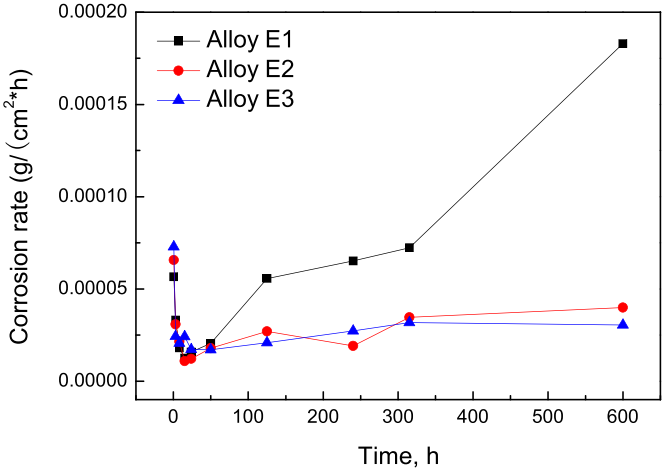

Fig. 7. Corrosion rate of alloy E1, E2 and E3 during immersion test.

c axis is perpendicular to the tensile stress, therefore extension twin would be inhibited and contraction twin would be promoted [24,25]. For alloy E2, there are also large amount of LAGBs in the grains after tensile test. It should be noticed that in some of the grains, LAGBs are distributed along straight lines, as indicated in Fig. 5 (g). These straight lines are considered to be slip bands. There are only a small amount of twins in alloy E2 after tensile test, which means that twinning is not the main deformation mode for alloy E2. These twins are mainly contraction twins, as revealed in Fig. 5 (h). There are few LAGBs and twins in alloy E3 after tensile test, as in Fig. 5 (k) and (l).

The microstructure evolution of alloy E1 and E2 during in-situ tensile test are shown in Fig. 6. As exhibited in Fig. 6 (a), there are almost no twins and slip bands in alloy E1 at the beginning of the tensile test. As the tensile deformation increase, twins appear in the unDRXed grains, and slip band can be found in the DRXed grains, as in Fig. 6 (b). At the last stage of tensile test, cracks form along twin boundaries in the unDRXed grains and at the grain boundaries where the slip band accumulates, as indicated in Fig. 6 (c). While for alloy E2, there are no unDRXed grains, and the main deformation mode is dislocation slip. As shown in Fig. 6 (d), there is almost no slip band in alloy E2 at the beginning of tensile test. As tensile deformation increase, slip bands are formed and increase, and then at the last stage of the tensile test, large numbers of slip bands can be found and accumulate at the grain boundaries, which caused cracks. It should be noted that secondary phases would also hinder the dislocation slip, so that the slip bands would also pile up at the interface between secondary phases and the matrix, thus cause cracks, as revealed in Fig. 6 (e) and (f).

According to the above analysis, the influence of extrusion process on the tensile property of Mg–Zn–Y-Nd alloy can be discussed from the following aspects of grain size, texture and secondary phases.

Firstly, it is widely known that grain refinement would increase the strength and ductility of alloy [26]. As shown in Fig. 1 and Table 2, the increase of extrusion ratio has increased the DRXed grain size, which would decrease the strength and ductility of the alloy. The increase of extrusion pass has refined the DRXed grains and increased the volume fraction of DRXed grains, which increases the strength and ductility obviously by the grain refinement effect.

Secondly, it is known that basal slip and extension twin would occur more easily during tensile test at room temperature because of their low CRSS values [24]. For the grains with basal texture, when the alloy is tensile tested along ED, the Schmid factor of basal slip and extension twin is 0. So that basal texture would prevent basal slip and extension twin, and lead to texture strengthening in the alloy. Comparing alloy E1, E2 and E3, the basal texture of alloy E1 is stronger than alloy E2, but weaker than alloy E3. Therefore it can be deduced that in the present study, the increase of extrusion ratio has reduced the texture strengthening effect of Mg–Zn–Y-Nd alloy, thus basal slip would become easier to be activated, and many slip band can be found in alloy E2 after tensile test. The TYS and TUS are decreased but the elongation increase significantly. The increase of extrusion pass has improved the texture strengthening effect, and basal slip would become harder to be activated. As a result, the TYS and TUS increases obviously but the elongation would decrease.

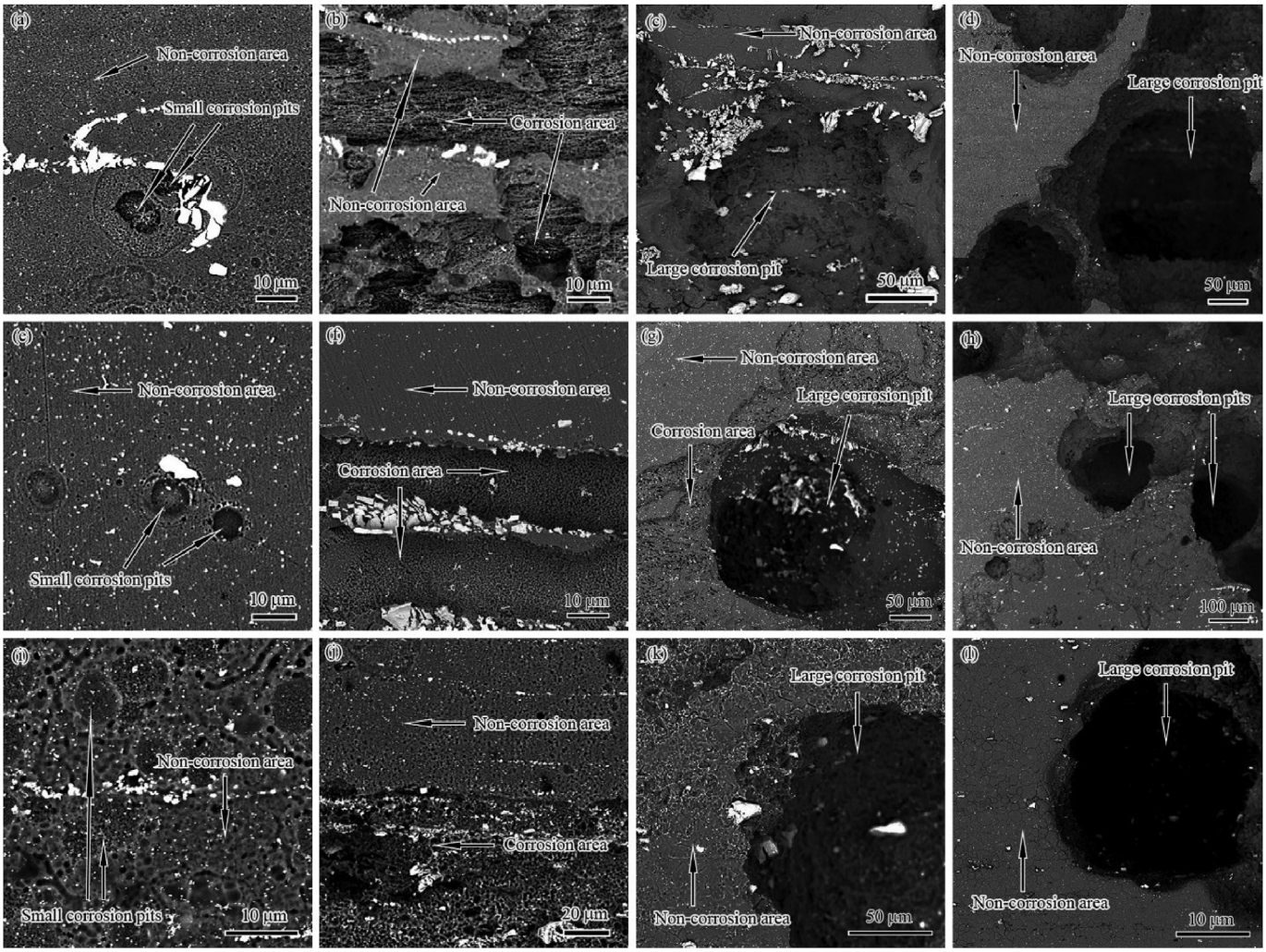

Fig. 8. The surface morphology of alloy E1, E2 and E3 after immersion for different time: (a) (b) (c) (d) Alloy E1; (e) (f) (g) (h) Alloy E2; (i) (j) (k) (l) Alloy E3; (a) (e) (i) 3 h; (b) (f) (j) 50 h; (c) (g) (k) 125 h; (d) (h) (l) 600 h.

Thirdly, the secondary phases would strengthen Mg alloys through impeding dislocation movement according to Orowan mechanism, and the precipitation strengthening effect can be described by Euq. 2 [27]:

$$\Delta\sigma_{ps} = M\frac{Gb}{2\pi\sqrt{1-v}}\frac{1}{\bar{d}\left(\sqrt{\frac{\pi}{4f-1}}\right)}ln\frac{\bar{d}}{b} \quad (1)$$

Where $\Delta\sigma_{ps}$ represents precipitation strengthening content, M, G and v are material constants, b is the burger vector (0.32 nm), f is the volume fraction of the secondary phases and $\bar{d}$ is the average size of the secondary phases. In the present study, the volume fractions of secondary phases are basically the same for these three alloys. Thus the difference of the precipitation strengthening effect among the three alloys is determined by $\bar{d}$. As exhibited in Table 2, the increase of extrusion ratio and pass would both refine the secondary phases, thus improve the precipitation strengthening effect of Mg–Zn–Y-Nd alloy.

In conclusion, the increase of extrusion ratio would increase the grain size, weaken the basal texture and refine the secondary phases, thus decrease the strength but increase the ductility of Mg–Zn–Y-Nd alloy. The increase of extrusion pass would refine the grains and secondary phases, and strengthening the basal texture, as a result, both the strength and ductility are improved.

3.3. Degradation performance

The Mg–Zn–Y-Nd alloys with different states were immersed in the Hank's solution at 37 °C for different time, and the corrosion rate was calculated according to the following equation.

$$CR = \frac{\Delta W}{At} \quad (2)$$

Where CR is the corrosion rate, ΔW is the weight loss, A is the surface area of the specimen, t is the immersion time. The corrosion rate of the alloys at different time is shown in Fig. 7. It can be found that the corrosion rate decrease at the beginning stage of immersion test for all of these three alloys. After immersion for about 24 h, the corrosion rate continues to increase for alloy E1. While for alloy E2, the corrosion rate presents a fluctuation trend, but on the whole, the corrosion rate does not change much after immersion for 24 h. For alloy E3, the corrosion rate rise quite slowly during immersion from 24 h to 315 h, and then drops slightly at 600 h. Comparing the corrosion rate of these three alloys, it can be found that the corrosion rate of alloy E1 is much higher than alloy E2 and E3. The corrosion rate of alloy E2 and E3 are very close. Accordingly, it can be concluded that the increase of extrusion ratio and pass have both improved the corrosion resistance of Mg–Zn–Y-Nd alloy, and their improvement effect are similar in the present study.

The surface morphologies of the samples after immersion for different time are observed through SEM and the results are shown in Fig. 8. The corrosion process of Mg–Zn–Y-Nd alloys in the present study can be described as follows: At the beginning of the corrosion process,

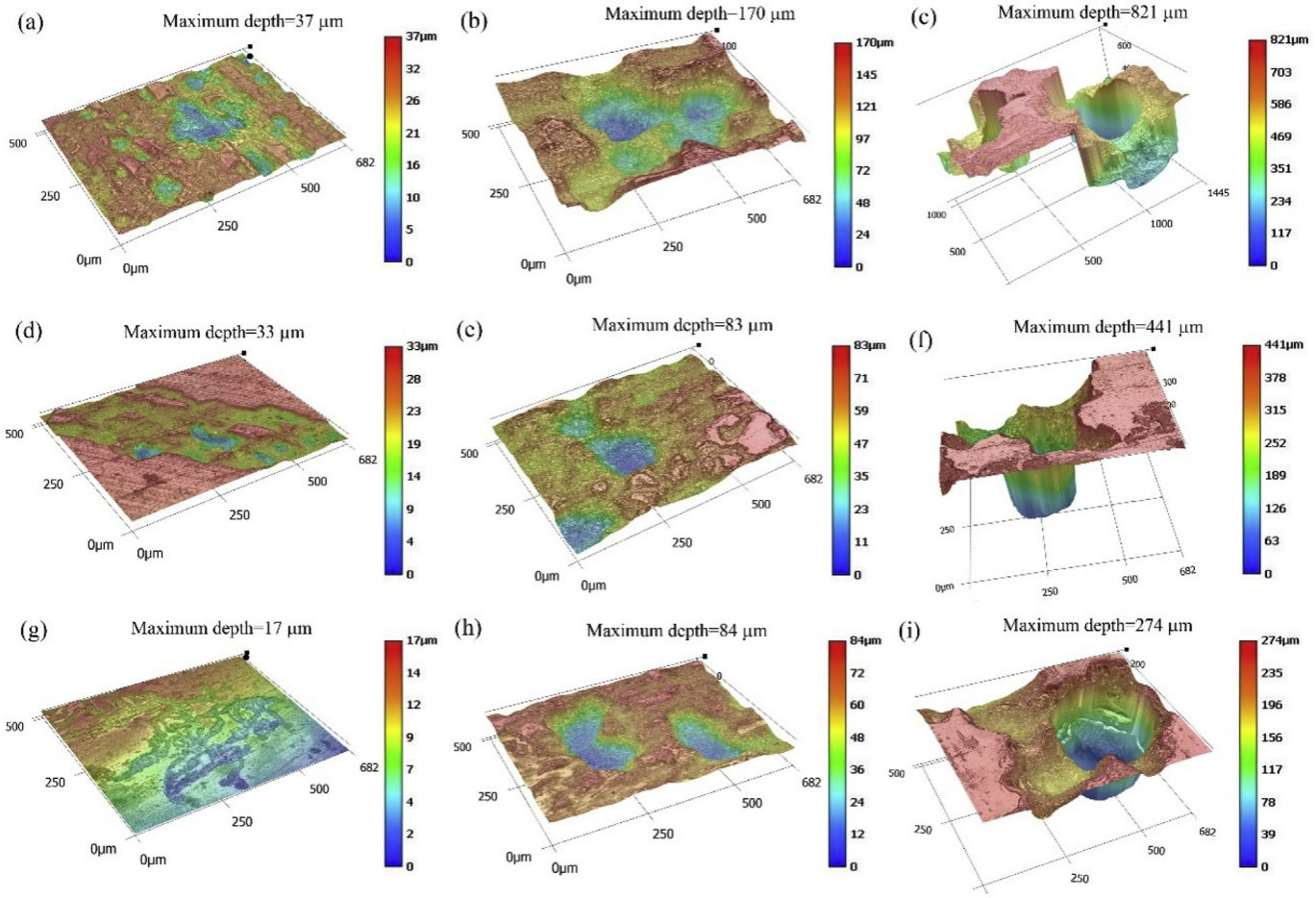

Fig. 9. The surface 3D morphology of alloy E1, E2 and E3 after immersion for different time: (a) (b) (c) Alloy E1; (d) (e) (f) Alloy E2; (g) (h) (i) Alloy E3; (a) (d) (g) 50 h; (b) (e) (h) 125 h; (c) (f) (j) 600 h.

small corrosion pits about dozens of microns appear. As the immersion time increase, the small corrosion pits increase and then expand along secondary phases and form strip corrosion area. After that, deep corrosion pits larger than 100 μm appear, which cause large weight loss. Then the large corrosion pits increase and become deeper. Comparing the corrosion morphology of these three alloys, it can be found that the corrosion of alloy E2 and E3 is not as serious as alloy E1.

From the surface morphologies of the samples after immersion, it can be deduced that the corrosion rate decrease at the beginning stage of immersion for the three alloys (immersion time less than 24 h) in Fig. 7 are caused by the continue formation of small corrosion pits that are covered by corrosion products, and these corrosion products could prevent further corrosion of the alloy, thus reduced the surface area in contact with Hank's sulution. As the immersion time increase, the corrosion area expands and the corrosion product segreagte and then falls off, exposing the Mg alloy surface resulting in an increase in the surface area of the alloy in contact with Hank's sulution. Therefore the corrosion rate starts to increase. As the immersion time continue to increase, the formation of large corrosion pits would further increase the corrosion rate, especially for alloy E1.

The surface 3D morphology of the samples after immersion for different time are observed and the results are shown in Fig. 9. The deepth of the corrosion pits can be measured. It is indicated that the small corrosion pits formed at the early stage of corrosion is about dozens of microns deepth, while the large corrosion pits formed at the later stage of corrosion could reach hundreds of microns. The corrosion pits of alloy E2 and E3 are shallower than alloy E1.

According to the above microstructure analysis, the increase of extrusion ratio could increase the volume fraction of DRXed grains, and result in complete recrystallization in alloy E2, thus leads to more uniform grains. It has been reported that the more uniform grains would result in decreased general corrosion rate and alleviation of corrosion localization [17]. Besides, the increase of extrusion ratio has refined the secondary phases. During immersion, the secondary phases would cause galvanic corrosion because of its more positive corrosion potential than the matrix, thus the matrix around the secondary phases would be corroded [28][29]. As the secondary phases distribute linearly along ED after thermal extrusion, the corrosion pits would locate along the secondary phase chains. The secondary phase refinement would decrease the galvanic corrosion pit size, and thus decrease the corrosion rate.

By increasing the extrusion pass, the grains and secondary phases become finer and more uniform. It is known that the small grain size creates more grain boundaries that act as a corrosion barrier to increase the corrosion resistance. Therefore the grain refinement and homogenization would improve the corrosion resistance of Mg–Zn–Y-Nd alloy in the present study. In addition, the secondary phases are also refined through increase of extrusion pass, which would also improve the corrosion performance of Mg–Zn–Y-Nd alloy.

4. Conclusions

In the present research, a biodegradable Mg–4Zn-1.2Y-0.8Nd alloy was fabricated and processed with different thermal extrusion processes. The microstructure, tensile property and corrosion behavior were characterized and analyzed to clarify the effect of extrusion ratio

and extrusion pass on the alloy. The results can be concluded as follows:

(1) The increase of extrusion ratio has increased the size and volume fraction of DRXed grains in the alloy. The increase of extrusion pass has increased the volume fraction but decreased the size of DRXed grains in the alloy. Both the increase of extrusion ratio and extrusion pass has refined the secondary phases.
(2) The increase of extrusion ratio has reduced the TYS and TUS, but increased the elongation of the alloy significantly. While the increase of extrusion pass has improved the TYS and TUS of the alloy greatly, but only slightly increased its elongation.
(3) Both the increase of extrusion ratio and extrusion pass has improved the corrosion resistance of the alloy obviously, and their reduction effects on the corrosion rate of the alloy are roughly the same.

CRediT authorship contribution statement

Beining Du: Conceptualization, Methodology, Investigation, Writing - original draft. **Ziyang Hu:** Investigation. **Jiali Wang:** Writing - review & editing. **Liyuan Sheng:** Investigation. **Hui Zhao:** Investigation. **Yufeng Zheng:** Writing - review & editing. **Tingfei Xi:** Writing - review & editing.

Declaration of competing interest

The authors declared that they have no conflicts of interest to this work. We declare that we do not have any commercial or associative interest that represents a conflict of interest in connection with the work submitted.

Acknowledgements

The authors are grateful to the National Key Research and Development Program of China (No. 2018YFC1106702), the Natural Science Foundation of Guangdong Province, China (No. 2018A030313950) and Shenzhen Basic Research Project (JCYJ20170815153143221 and JCYJ20170815153210359) for financial support.

References

[1] R. Zeng, W. Dietzel, F. Witte, N. Hort, C. Blawert, Progress and challenge for magnesium alloys as biomaterials, Adv. Eng. Mater. 10 (2008) 3–14.
[2] J. Vormann, Magnesium: nutrition and metabolism, Mol. Aspect. Med. 24 (2003) 27–37.
[3] Y. Zheng, X. Gu, F. Witte, Biodegradable metals, Mater. Sci. Eng. R. 77 (2014) 1–34.
[4] R. Huiskes, H. Weinans, B. Van Rietbergen, The relationship between stress shielding and bone resorption around total hip stems and the effects of flexible materials, Clin. Orthop. Relat. Res. (1992) 124–134.
[5] M.P. Staiger, A.M. Pietak, J. Huadmai, G. Dias, Magnesium and its alloys as orthopedic biomaterials: a review, Biomaterials 27 (2006) 1728–1734.
[6] Z. Li, X. Gu, S. Lou, Y. Zheng, The development of binary Mg–Ca alloys for use as biodegradable materials within bone, Biomaterials 29 (2008) 1329–1344.
[7] A. Witecka, A. Bogucka, et al., In vitro degradation of ZM21 magnesium alloy in simulated body fluids, Mater. Sci. Eng. C 65 (2016) 59–69.
[8] J. WKang, C.J. Wang, K.K. Deng, K.B. Nie, Y. Bai, W.J. Li, Microstructure and mechanical properties of Mg-4Zn-0.5Ca alloy fabricated by the combination of forging, homogenization and extrusion process, J. Alloys Compd. 720 (2017) 196–206.
[9] J. Lin, Q. Wang, L. Peng, H.J. Roven, Microstructure and high tensile ductility of ZK60 magnesium alloy processed by cyclic extrusion and compression, J. Alloys Compd. 476 (2009) 441–445.
[10] X.B. Zhang, G.Y. Yuan, J.L. Niu, P.H. Fu, W.J. Ding, Microstructure, mechanical properties, biocorrosion behavior, and cytotoxicity of as-extruded Mg–Nd–Zn–Zr alloy with different extrusion ratios, J. Mech. Behav. Biomed. 9 (2012) 153–162.
[11] K. Liu, C.C. Sun, et al., Microstructure, texture and mechanical properties of Mg–Zn–Er alloys containing I-phase and W-phase simultaneously, J. Alloys Compd. 665 (2016) 76–85.
[12] S.H. Allameh, M. Emamy, E. Maleki, B. Pourbahari, Effect of microstructural refinement on tensile properties of AZ80 magnesium alloy via Ca addition and extrusion process, Proc. Mater. Sci. 11 (2015) 89–94.
[13] Q. Chen, J. Lin, D. Shu, C. Hu, Z. Zhao, F. Kang, et al., Microstructure development, mechanical properties and formability of Mg–Zn–Y–Zr magnesium alloy, Mater. Sci. Eng. 554 (2012) 129–141.
[14] Z.D. Zhao, Q. Chen, L. Yang, D.Y. Shu, Z.X. Zhao, Microstructure and mechanical properties of Mg-Zn-Y-Zr alloy prepared by solid state recycling, Trans. Nonferrous Metals Soc. China 21 (2011) 265–271.
[15] Q. Chen, D. Shu, Z. Zhao, Z. Zhao, Y. Wang, B. Yuan, Microstructure development and tensile mechanical properties of Mg–Zn–RE–Zr magnesium alloy, Mater. Des. 40 (2012) 488–496.
[16] Y. Tian, H. Huang, G. Yuan, W. Ding, Microstructure evolution and mechanical properties of quasicrystal-reinforced Mg–Zn–Gd alloy processed by cyclic extrusion and compression, J. Alloys Compd. 626 (2015) 42–48.
[17] Q. Wu, S.J. Zhu, L. GWang, Q. Liu, G.C. Yue, J. Wang, S.K. Guan, The microstructure and properties of cyclic extrusion compression treated Mg–Zn–Y–Nd alloy for vascular stent application, J. Mech. Behav. Biomed. 8 (2012) 1–7.
[18] B.N. Du, Z.P. Xiao, Y.X. Qiao, L. Zheng, B.Y. Yu, D.K. Xu, et al., Optimization of microstructure and mechanical property of a Mg-Zn-Y-Nd alloy by extrusion process, J. Alloys Compd. 775 (2019) 990–1001.
[19] X. Xu, X. Chen, W. Du, Y. Geng, F. Pan, Effect of Nd on microstructure and mechanical properties of as-extruded Mg-Y-Zr-Nd alloy, J. Mater. Sci. Technol. 33 (2017) 926–934.
[20] Y. Chen, Q. Wang, J. Peng, C. Zhai, W. Ding, Effects of extrusion ratio on the microstructure and mechanical properties of AZ31 Mg alloy, J. Mater. Process. Technol. 182 (2007) 281–285.
[21] Y. Uematsu, K. Tokaji, M. Kamakura, K. Uchida, H. Shibata, N. Bekku, Effect of extrusion conditions on grain refinement and fatigue behaviour in magnesium alloys, Mater. Sci. Eng. 434 (2006) 131–140.
[22] M. Hirano, M. Yamasaki, K. Hagihara, K. Higashida, Y. Kawamura, Effect of extrusion parameters on mechanical properties of Mg97Zn1Y2 alloys at room and elevated temperatures, Mater. Trans. 51 (2010) 1640–1647.
[23] J.P. Hadorn, K. Hantzsche, S. Yi, J. Bohlen, D. Letzig, J.A. Wollmershauser, et al., Role of solute in the texture modification during hot deformation of Mg-rare earth alloys, Metall. Mater. Trans. 43 (2012) 1347–1362.
[24] S.G. Hong, S.H. Park, C.S. Lee, Role of {10–12} twinning characteristics in the deformation behavior of a polycrystalline magnesium alloy, Acta Mater. 58 (2010) 5873–5885.
[25] N.S. Prasad, N. Naveen Kumar, R. Narasimhan, S. Suwas, Fracture behavior of magnesium alloys – role of tensile twinning, Acta Mater. 94 (2015) 281–293.
[26] Y. Du, M. Zheng, X. Qiao, K. Wu, X. Liu, G. Wang, et al., The effect of double extrusion on the microstructure and mechanical properties of Mg–Zn–Ca alloy, Mater. Sci. Eng. 583 (2013) 69–77.
[27] W.J. Li, K.K. Deng, X. Zhang, K.B. Nie, F.J. Xu, Effect of ultra-slow extrusion speed on the microstructure and mechanical properties of Mg-4Zn-0.5 Ca alloy, Mater. Sci. Eng. 677 (2016) 367–375.
[28] W. Zhou, T. Shen, N.N. Aung, Effect of heat treatment on corrosion behaviour of magnesium alloy AZ91D in simulated body fluid, Corrosion Sci. 52 (2010) 1035–1041.
[29] B. Du, Z. Hu, L. Sheng, et al., Influence of Zn Content on Microstructure and Tensile Properties of Mg–Zn–Y–Nd Alloy, Acta Metallurgica Sinica (English Letters) 31 (4) (2018) 351–361.